Hindawi
Advances in Meteorology
Volume 2018, Article ID 7301314, 13 pages
https://doi.org/10.1155/2018/7301314

Research Article

ESA CCI Soil Moisture Assimilation in SWAT for Improved Hydrological Simulation in Upper Huai River Basin

Yongwei Liu[1], **Wen Wang**[2], **and Yuanbo Liu**[1]

[1] *Key Laboratory of Watershed Geographic Sciences, Nanjing Institute of Geography & Limnology, Chinese Academy of Sciences, Nanjing 210008, China*
[2] *State Key Laboratory of Hydrology-Water Resources and Hydraulic Engineering, Hohai University, Nanjing 210098, China*

Correspondence should be addressed to Yuanbo Liu; ybliu@niglas.ac.cn

Received 12 February 2018; Revised 1 May 2018; Accepted 16 May 2018; Published 7 June 2018

Academic Editor: Stefano Dietrich

The assimilation of satellite soil moisture (SM) products with coarse resolution is promising in improving rainfall-runoff modeling, but it is largely impacted by the data assimilation (DA) strategy. This study performs the assimilation of a satellite soil moisture product from the European Space Agency (ESA) Climate Change Initiative (CCI) in a physically based semidistributed hydrological model (SWAT) in the upper Huai River basin in China, with the objective to improve its rainfall-runoff simulation. In this assimilation, the ensemble Kalman filter (EnKF) is adopted with full consideration of the model and observation error, the rescaling technique for satellite SM, and the regional applicability of the hydrological model. The results show that the ESA CCI SM assimilation generally improves the streamflow simulation of the study catchment. It is more effective for low-flow simulation, while for very high-flow/large-flood modeling, the DA performance shows uncertainty. The less-effective performance on large-flood simulation lies in the relatively low dependence of rainfall-runoff generation on the antecedent SM as during which the SM is nearly saturated and the runoff is largely dominated by precipitation. Besides, the efficiency of DA is deteriorated by the dense forest coverage and the complex topography conditions of the basin. Overall, the ESA CCI SM assimilation improves the streamflow simulation of the SWAT model in particular for low flow. This study provides an encouragement for the application of the ESA CCI SM in water management, especially over low-flow periods.

1. Introduction

Soil moisture (SM) significantly impacts the rainfall-runoff process as it dominates the partitioning of precipitation into infiltration, runoff, and evaporation. In recent years, a large body of studies have been implemented to explore the approaches to improving rainfall-runoff modeling via enhancing SM estimation [1–10].

One promising approach to improving SM estimation in turn improving rainfall-runoff modeling is to integrate the observed SM into the hydrological modeling process using data assimilation (DA) techniques [11–16]. In general, the SM data for integration can be obtained from field measurements and satellite observations. The in situ measurements are insufficient in the availability and spatial representativeness due to the high spatial heterogeneity of SM. Major researches on in situ SM assimilation focus on discussing the DA approaches and exploring the potential of SM assimilation in improving the hydrological process [13, 17, 18]. However, the satellite observations are capable of capturing the spatial distribution and temporal dynamics of SM on large scales. Despite the fact that the satellite remote sensing (RS) can only detect the surface SM information with a few centimeters (~5 cm), it could represent the fastest response of SM dynamics to meteorological conditions [19]. A large number of studies have been implemented to assimilate the RS SM in the land surface model for the purpose of obtaining a more accurate and reliable profile SM data set on a regional or global scale [20–26]. Nevertheless, the assimilation of coarse-scale RS SM in the hydrological model targeted at improving the rainfall-runoff process is implemented in relatively few studies [10, 27–31]. Currently, there is still no consensus on the improvement of streamflow modeling through satellite

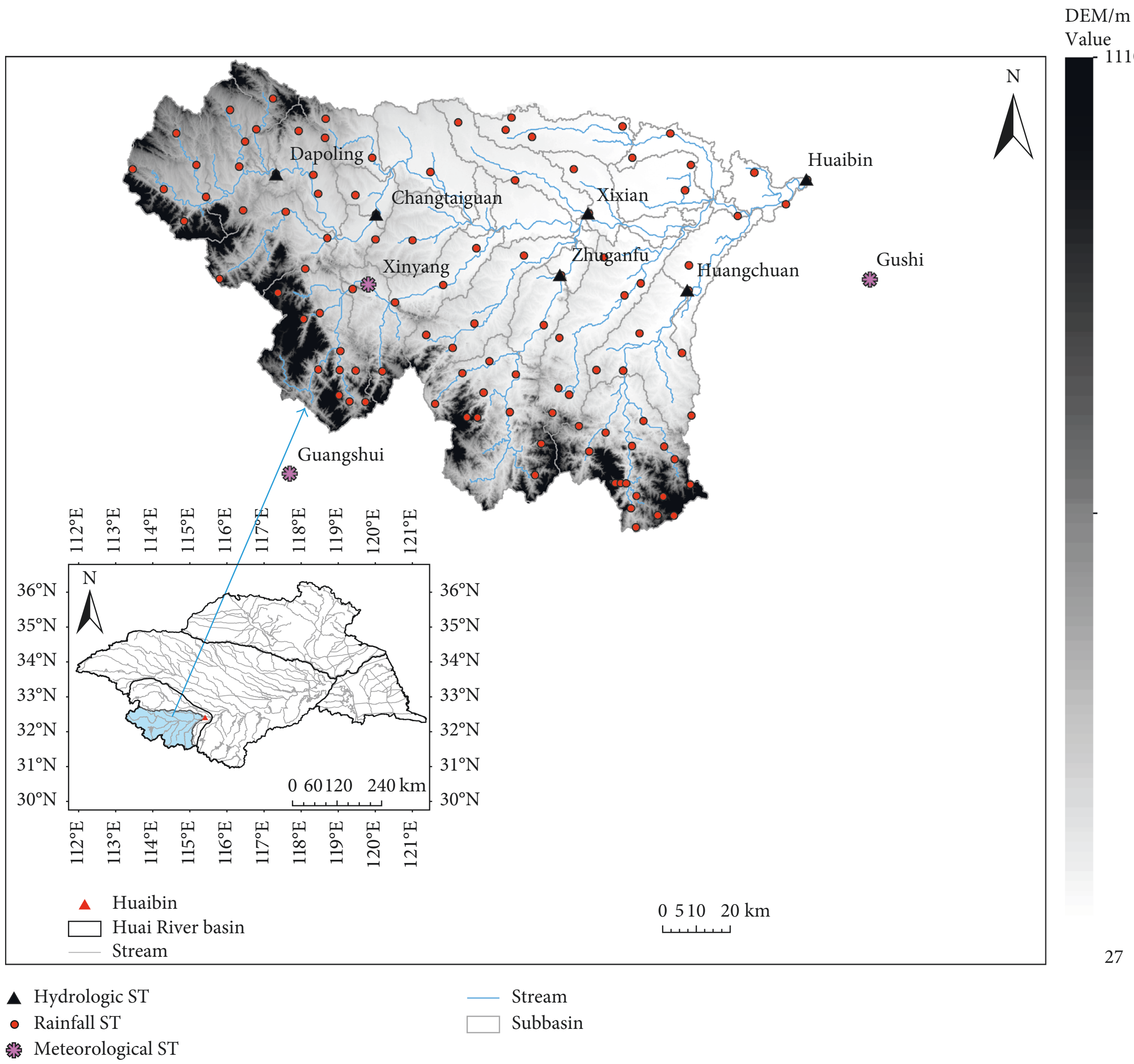

Figure 1: The upper Huai River basin: location (the inset map), elevation, digital river network, location of the meteorological and hydrological stations (ST), and the subbasin delineation in SWAT model building.

soil moisture assimilation [4, 7]. For instance, almost no improvement of streamflow simulation was obtained by Brocca et al. [4] in the assimilation of the surface ASCAT SM retrievals, while up to 10–30% improvements were achieved in such other studies as Massari et al. [32], Lopez et al. [7], and Loizu et al. [10]. The large discrepancies of the DA performance in previous studies are likely due to the fact that it is influenced by various factors in the DA framework setup, such as the quantification of the model and observation error, the mismatch between the observed and simulated SM, the data quality and rescaling technique for RS SM, and the model physical mechanism and its regional applicability. To date, the added value of satellite soil moisture data in hydrological modeling is still underexplored [5, 32]. The performance of RS soil moisture assimilation in streamflow modeling presents certain specificity on the satellite data itself, the hydrological model, and the different configuration schemes in the DA framework setup. Therefore, specific studies on satellite soil moisture assimilation with comprehensive consideration of the DA implementation strategies are essential for exploring the significance of satellite soil moisture in hydrological modeling.

In this paper, a case study for satellite soil moisture assimilation is implemented in the upper Huai River basin in China, with full consideration of the factors in the DA framework including the quantification of the model and observation error, the rescaling technique for RS SM, and the regional applicability of the hydrological model. This data assimilation is performed in a physically based semi-distributed hydrological model (SWAT) based on a robust sequential data assimilation approach (the ensemble Kalman filter (EnKF)). A multisatellite-merged soil moisture data set from the European Space Agency (ESA) Climate Change Initiative (CCI) is adopted as the assimilation data source.

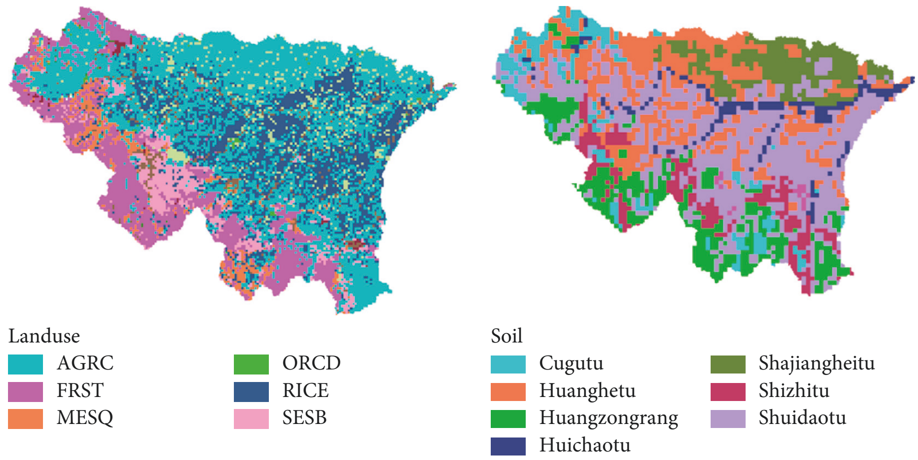

Figure 2: Land use/land cover (LU/LC) classes and soil distribution for the upper Huai River basin.

The main objective of this study is to explore the potential of coarse-scale RS soil moisture in improving runoff modeling and to provide recommendations on the assimilation strategy.

2. Study Area and Data Used

2.1. Study Area. The study catchment is located in the upstream basin of the Huaibin hydrologic station in the Huai River basin, China (Figure 1). The watershed covers about 16000 km^2. The whole watershed is located in the transition region between the northern subtropical zone and the warm temperate zone. Its annual average rainfall is around 900 mm, 50%–80% of which falls during June to September. Here, the annual average temperature is about 15°C. The major land cover is the agriculture land (AGRC 32.5%, RICE 35%) and forest (FRST 23.6%) (Figure 2).

2.2. Data for SWAT Model. SWAT model building requires meteorological and underlying surface data. The meteorological data mainly include precipitation, maximum and minimum temperature, solar radiation, wind speed, and relative humidity. The precipitation data are drawn from 106 local rainfall stations within the catchment (Figure 1). The other five meteorological data come from the three meteorological gauges (Xinyang, Gushi, and Guangshui) (Figure 1). The underlying surface data are the digital elevation (DEM), land cover, and soil category data. The DEM data are downloaded from the Shuttle Radar Topography Mission with a spatial resolution of 90 m (http://datamirror.csdb.cn/index.jsp). The land use/land cover (LU/LC) data are collected from the Chinese Cold and Arid Regions Science Data Center (http://westdc.westgis.ac.cn/) with a spatial resolution of 1 km (Figure 2). The soil data are resampled from a soil map at a scale of 1 : 100000 from the Soil Handbook of Henan Province. The soil for the whole catchment is divided into seven categories (Figure 2). The soil texture and its corresponding United States Department of Agriculture (USDA) classification for each category are shown in Table 1. Besides, there are six hydrologic stations (Dapoling, Changtaiguan, Zhuganfu, Xixian, Huangchuan, and Huaibin) (Figure 1) with daily streamflow measurements of 1992–2008 (the data quality issue exists for the years 2000 and 2001) in this basin.

2.3. ESA CCI Soil Moisture Data. The ESA CCI soil moisture data are a merged multisatellite surface soil moisture product developed in the Climate Change Initiative (CCI) by the European Space Agency (ESA). It combines the soil moisture retrievals from four microwave radiometers (SMMR, SSM/I, TMI, and AMSR-E) and two scatterometers (AMI and ASCAT) into a 0.25° global daily data set over 30 years from 1978. The data integration relies on their respective sensitivity to vegetation density and uses a Noah GLDAS-1 surface soil moisture product [33] as a climatology reference [34]. The ESA CCI SM consists of active, passive, or combined products. The active/passive products are the integration of the scatterometer/radiometer-based SM retrievals, respectively, while the combined product is the fusion of both the active and passive products. In this study, the combined product (ESA CCI SM v03.2) is adopted for soil moisture assimilation.

3. Methodology

3.1. Soil and Water Assessment Tool (SWAT). The SWAT is a physically based semidistributed watershed model, which has been widely used in rainfall-runoff modeling over recent years [35, 36]. In hydrological modeling, the catchment is firstly delineated into several subbasins according to its topography. Then, each subbasin is further divided into several hydrological response units (HRUs) based on the land use, soil, and slope. HRUs are basic calculation units for the land phase of the hydrologic cycle, on which the processes for surface runoff, lateral flow, and ground water are generated accompanied by evapotranspiration and soil water routing.

Soil moisture lies in the center of the hydrologic cycle and makes different impacts on the above process. The initial profile soil water content influences surface runoff generation through the curve number in the SCS method [37]. After surface runoff generation, the water infiltrated to the

Table 1: Soil classification and its area proportions in the upper Huai River basin.

Soil category	Clay (%)	Silt (%)	Sand (%)	Rock (%)	USDA soil texture	Soil layer (mm)	Area proportion (%)
Cugutu	7.05	34	35.9	23.1	Sandy loam	0-50-150	7.35
Huanghetu	23.43	65.1	11.5	0	Silt loam	0-50-150-400-800	21.52
Huangzongrang	17.03	39.4	43.6	0	Loam	0-50-150-400-800	13.7
Huichaotu	12.86	51.8	35.3	0	Silt loam	0-50-150-400-800	4.72
Shajiangheitu	20.32	65.5	14.2	0	Silt loam	0-50-150-400-800	9.81
Shizhitu	9.16	44.1	46.7	0	Loam	0-50-150	7.8
Shuidaotu	16.46	71	12.5	0	Silt loam	0-50-150-400-800	34.62

soil profile is redistributed based on a storage routing technique with the soil water field capacity as the threshold. The water balance for each soil layer can be expressed as follows:

$$\mathrm{SW}'_{\mathrm{ly}} = \mathrm{SW}_{\mathrm{ly}} + \Delta w_{\mathrm{perc,ly}} - Q_{\mathrm{lat,ly}} - E_{\mathrm{a,ly}}, \quad (1)$$

where $\mathrm{SW}_{\mathrm{ly}}$ and $\mathrm{SW}'_{\mathrm{ly}}$ are the soil water content (mm) at the start and end of the day, $\Delta w_{\mathrm{perc,ly}}$ is the net percolation from the overlying layer (i.e., the layer ly + 1), $Q_{\mathrm{lat,ly}}$ is the lateral flow generated from the layer ly, and $E_{\mathrm{a,ly}}$ is the evapotranspiration drawn from the layer ly.

The evapotranspiration from soil mainly includes two parts: soil evaporation and plant uptake/transpiration. In the SWAT, the potential evapotranspiration is firstly calculated using the Penman–Monteith equation [38]. Based on the potential evapotranspiration, the leaf area index, and the aboveground biomass and residue conditions, both the demand for transpiration/plant uptake and the demand for soil evaporation are determined. Then, the soil evaporation demand and the plant uptake demand for each soil layer are estimated using a depth distribution function. Finally, relying on the soil evaporation demand and the plant uptake demand with the available soil water as a constraint, the actual soil water evaporation and plant uptake are determined. In the processes mentioned above, the actual soil water extraction of a given layer is not allowed to be compensated by the extraction from other layers. However, the soil water deficiency can be made up by adjusting the soil compensation (*esco*) and plant compensation (*epco*) factors via changing the depth distribution of the soil evaporation demand and the plant water uptake demand. Besides, the calculation for the soil water percolation ($w_{\mathrm{perc,ly}}$) and lateral flow ($Q_{\mathrm{lat,ly}}$) is [39] omitted here.

In the water routing phase, the SWAT adopts a storage feature to calculate the surface runoff and lateral flow generated from each HRU to the main channel, while it applies a linear reservoir similar technique to account for the ground water to the main channel. The channel water routing is performed using a variable storage routing method [40].

3.2. The Ensemble Kalman Filter (EnKF) for Soil Moisture Assimilation. The EnKF is a sequential DA approach evolved from the standard Kalman filter [41]. It is based on an ensemble of model states produced by adding the Monte Carlo noise to model forcing and states and/or parameters to approximate the model state error covariance matrix for the purpose of optimally merging the model predictions with observations.

The state ensemble forecast at time t can be expressed as follows:

$$X_t^{\mathrm{f}} = F\left(X_{t-1}^{\mathrm{u}}, u_t, \delta\right) + \omega_t w_t \sim N\left(0, \sigma_{\mathrm{s}}^2\right), \quad (2)$$

where X_t^{f} is the forecasted state ensemble at time t and X_{t-1}^{u} is the updated state ensemble at $t-1$. In this study, it is constructed by the profile SM with up to four layers (Table 1) for all HRUs of the study basin (the HRUs delineation is detailed in Section 3.1). u_t represents the model forcing inputs. In this study, it mainly includes the observed precipitation P and temperature T at each site. The precipitation error is assumed to be independent both in time and in space; that is, both the autocorrelation between time steps at each rainfall station and the error correlation among different stations are ignored. The perturbation (η_{p}) to precipitation is assumed to be a lognormal multiplicative distribution with mean 1 and covariance σ_{p}^2 (3). The perturbation to temperature (η_{T}) is assumed to be an additive normal distribution with mean 0 and covariance σ_{T}^2 (4). Besides, δ represents the model parameter with a perturbation (η_{par}) of normal multiplicative distribution of mean 1 and covariance σ_{par}^2 (5). ω_{t} is the stochastic perturbation to the forecasted SM, being assumed to be an additive normal distribution with mean 0 and covariance σ_{s}^2:

$$P_{\mathrm{e}} = P \cdot \eta_{\mathrm{p}}, \quad \eta_{\mathrm{p}} \sim \ln N\left(1, \sigma_{\mathrm{p}}^2\right), \quad (3)$$

$$T_{\mathrm{e}} = T + \eta_{\mathrm{T}}, \quad \eta_{\mathrm{T}} \sim N\left(0, \sigma_{\mathrm{T}}^2\right), \quad (4)$$

$$\delta_{\mathrm{e}} = \delta \cdot \eta_{\mathrm{par}}, \quad \eta_{\mathrm{par}} \sim N\left(1, \sigma_{\mathrm{par}}^2\right). \quad (5)$$

The state update for soil moisture can be obtained by

$$X_t^{\mathrm{u}} = X_t^{\mathrm{f}} + K_t\left(Z_t - H\left(X_t^{\mathrm{f}}\right)\right), \quad (6)$$

where Z_t is the observation ensemble at time t. It is constructed by the RS SM for all grids covering the basin and being stochastically perturbed by an additive normal distribution with mean 0 and covariance σ_{R}^2. H is the observation operator, being used to map the model states to the observations. It is constructed by the area proportions of HRUs in RS grids as the SWAT model-simulated SM is on the HRU level, while the observed SM is on RS grids. K_t is the Kalman gain, which is calculated based on the forecast and observation error covariance:

$$K_t = P_{\mathrm{ms},t}\left(P_{\mathrm{s},t} + R_{\mathrm{s},t}\right)^{-1}, \quad (7)$$

where $P_{\mathrm{ms},t}$ is the cross-error covariance between the predicted SM (X_t^{f}) and the measurement prediction $H(X_t^{\mathrm{f}})$ at time t,

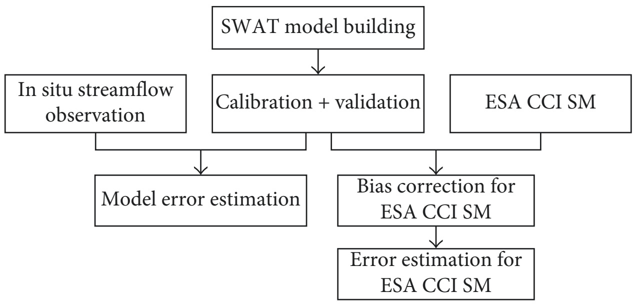

Figure 3: Flow chart for implementing ESA CCI SM assimilation in SWAT.

$P_{s,t}$ is the error covariance of the measurement prediction at time t, and $R_{s,t}$ is the error covariance of the RS SM at time t.

3.3. Implementation of the ESA CCI SM Assimilation in SWAT. To set up the ESA CCI SM data assimilation in the SWAT model, the SWAT model for the study catchment should be firstly built up. The model applicability is evaluated over the model calibration and validation processes. Then, the model error for the validated SWAT model is estimated based on the in situ streamflow observations at the Huaibin hydrologic station. Besides, the observation error estimation for the ESA CCI SM is implemented before the bias correction on the basis of the model-simulated soil moisture. A flow chart for implementing ESA CCI SM assimilation in SWAT is shown in Figure 3.

3.3.1. SWAT Calibration. The SWAT model for the upper Huai River basin is built up based on the meteorological forcing and land surface data (Section 2.2). This catchment is partitioned into 37 subbasins (Figure 1) and 146 hydrological response units (HRUs). To simplify and improve the model calibration process, a sensitivity analysis of the model parameters to the hydrologic modeling is implemented using the Latin-hypercube and one-factor-at-a-time method [42, 43]. Thereafter, the model is calibrated and validated using the daily runoff records over 1992–1999 and 2002–2008 at the interior and outlet hydrologic stations (i.e., Dapoling, Changtaiguan, Zhuganfu, Xixian, Huangchuan, and Huaibin in Figure 1), respectively. The parameter optimization is achieved by a combination of the autocalibration using the Sequential Uncertainty Fitting (SUFI2) [44] with the Nash–Sutcliffe coefficient of efficiency (detailed in Section 3.4) as the objective criteria and the manual fine-running method.

3.3.2. Model Error Estimation. The determination of the model error is significant for the performance of DA as the model predictions and observations are merged based on the relative weight between the model and observation error (as in (6) and (7)). In this study, the model error is mainly contributed by the model input error for precipitation and temperature, the model parameter error for parameters sensitive to SM simulation (e.g., the available soil water capacity), and the model state error for simulated SM. The various errors mentioned above are characterized by additive/multiplicative normal/lognormal distribution specified in Section 3.2. The assumed distribution is only controlled by the standard deviation (SD), that is, σ_{p}, σ_{T}, σ_{par}, and σ_{s} in (3), (4), (5), and (2), respectively. Therefore, the model error estimation is to quantify the model error parameters σ_{p}, σ_{T}, σ_{par}, and σ_{s}.

The quantification of σ_{p}, σ_{T}, σ_{par}, and σ_{s} is performed by analyzing the statistical characteristics of the simulated streamflow ensemble driven by model error perturbations on the basis of the observed streamflow at in situ sites. If the ensemble spread after perturbation is too large, the overfitting of observation exists in DA. Otherwise, the observed information cannot be fully utilized in DA. Therefore, the two ensemble verification measures (8) and (9) should be satisfied [32]. That is, if the ensemble spread sp is large enough, the temporal mean of the ensemble skill $\overline{sk}$ should be similar to the temporal average of the ensemble spread $\overline{sp}$:

$$\frac{\overline{sp}}{\overline{sk}} \cong 1. \tag{8}$$

And the observation should be indistinguishable from a member of the ensemble (N is the ensemble size):

$$\frac{\langle sk \rangle}{\langle mse \rangle} = \sqrt{\frac{N+1}{2N}}, \tag{9}$$

where

$$\begin{aligned}
\overline{sp} &= \frac{1}{T}\sum_{k}^{T}\left\{\frac{1}{N}\sum_{i=1}^{N}\left(Q_k^i - \overline{Q}_k\right)^2\right\},\\
\overline{sk} &= \frac{1}{T}\sum_{k=1}^{T}\left\{\left(\overline{Q}_k - Q_{\mathrm{obs},k}\right)^2\right\},\\
\langle sk \rangle &= \frac{1}{T}\sum_{k=1}^{T}\left|\overline{Q}_k - Q_{\mathrm{obs},k}\right|,\\
\langle \mathrm{mse} \rangle &= \frac{1}{T}\sum_{k=1}^{T}\left\{\frac{1}{N}\sum_{i=1}^{N}\left(Q_k^i - Q_{\mathrm{obs},k}\right)^2\right\}^{1/2},
\end{aligned} \tag{10}$$

where Q_k^i is the model simulated streamflow of the ensemble member i at time k, $\overline{Q}_k$ is the ensemble mean of the model simulated streamflow, $Q_{\mathrm{obs},k}$ is the observed streamflow at time k, and T is the total time step. Different $\overline{sp}/\overline{sk}$ and $\langle sk \rangle/\langle mse \rangle$ can be obtained with different σ_{p}, σ_{T}, σ_{par}, and σ_{s}, that is, $f(\sigma_{\mathrm{p}}, \sigma_{\mathrm{T}}, \sigma_{\mathrm{par}}, \sigma_{\mathrm{s}}) = \overline{sp}/\overline{sk}$ and $g(\sigma_{\mathrm{p}}, \sigma_{\mathrm{T}}, \sigma_{\mathrm{par}}, \sigma_{\mathrm{s}}) = \langle sk \rangle/\langle mse \rangle$. Therefore, the optimal estimation of σ_{p}, σ_{T}, σ_{par}, and σ_{s} can be realized by searching for the minimum value of the following function:

$$F = \sqrt{\left(f\left(\sigma_{\mathrm{p}}, \sigma_{\mathrm{T}}, \sigma_{\mathrm{par}}, \sigma_{\mathrm{s}}\right) - 1\right)^2 - \left(g\left(\sigma_{\mathrm{p}}, \sigma_{\mathrm{T}}, \sigma_{\mathrm{par}}, \sigma_{\mathrm{s}}\right) - \sqrt{(N+1)/2N}\right)^2}. \tag{11}$$

In the soil moisture assimilation, the temperature error (σ_T) is not very sensitive to DA performance. Hence, σ_T is set to be 1°C as referenced from the study of Chen et al. [12]. Besides, the predicted/simulated SM error σ_s is set to be 0.01 m^3/m^3 to avoid rapid changes of soil water content between continuous time steps [45, 46]. Finally, the precipitation (σ_p) and model parameter error (σ_{par}) are determined by searching for the minimum F based on the streamflow measurements at the catchment outlet (Huaibin station) over 2002–2004 with an ensemble size of 200.

3.3.3. ESA CCI SM Bias Correction. Remote sensing (RS) retrieval of SM often has systematic bias to the in situ observed and model-simulated soil moisture due to their large differences in spatial resolution and detection depth. The model-simulated SM can generally meet the water balance of the basin/region. In order to keep the basin's water balance in DA, the systematic bias in RS SM needs to be corrected before DA [47]. In this study, the bias correction for the ESA CCI SM uses the cumulative distribution function (CDF) approach [48], where the probability of the RS SM and the simulated SM is assumed to be the same. The spatial matching between them uses the area-weighted average method to aggregate the simulated SM from HRUs to RS grids. Here, the rescaling is performed over the complete model validation period of 2002–2008, considering that CDF estimation typically requires a long record of observed and model simulated data [6].

3.3.4. ESA CCI SM Error Estimation. Rational quantification on the uncertainty of RS SM is important for its optimal application. RS SM still has considerable uncertainty although its accuracy and reliability have been largely improved in recent years [49, 50]. In this study, referencing from previous researches [5, 51, 52], the error for ESA CCI SM is assumed to be an additive Gaussian distribution with the standard deviation (SD) of σ_R. Here, the estimation of σ_R is obtained from the equation referring to the study of Lievens et al. [30]:

$$\sigma_R = a_0 + b_0 \text{ sm\_uncertainty} + c_0 \text{ frc}, \tag{12}$$

where sm_uncertainty is an indicator of the data uncertainty for the ESA CCI SM [53, 54], which is not fully considered as the representativeness error (e.g., the error caused by vegetation or different layer depths). The representativeness error is accounted by the parameter a_0, which represents the minimum retrieval error for ESA CCI SM. frc is the fraction of the ESA CCI SM grid cell covered by the forest. The calculation of frc is based on the land cover data collected from the Chinese Cold and Arid Regions Science Data Center (http://westdc.westgis.ac.cn/) (Figure 2). a_0, b_0, and c_0 are given parameters, and $b_0, c_0 \in (0, 1)$. Referencing from the study of Lievens et al. [30], a_0, b_0, and c_0 are given as 0.02, 0.5, and 0.02, respectively, in this study. It should be noted that when the ESA CCI SM is high orderly rescaled (Section 3.3.3), the observation error parameter σ_R needs to be rescaled according to

$$\sigma_R^* = \frac{\sigma_{sim}}{\sigma_{obs}}\sigma_R, \tag{13}$$

where σ_R^* is the standard deviation (SD) of the rescaled ESA CCI SM observation error, and σ_{sim} and σ_{obs} are the SD of the simulated SM error and the ESA CCI SM error, respectively.

3.4. Evaluation Metrics. The relative error (RE), the root mean square error (RMSE), the Nash–Sutcliffe coefficient of efficiency (NSE), and Pearson's correlation coefficient (R) are used to measure the coincidence level of the simulated streamflow to the field observations. Meanwhile, the effectiveness criterion (EFF) [55] and the normalized error reduction index (NER) are used to directly assess the performance of soil moisture assimilation.

RE describes the deviation rate (%) of the predicted streamflow to its field measurements. It can be expressed by

$$\text{RE} = \frac{\sum_{i=1}^{n}\left(Q_i^{sim} - Q_i^{obs}\right)}{\sum_{i=1}^{n} Q_i^{obs}} \cdot 100\%, \tag{14}$$

where n is the total time step and Q_i^{sim} and Q_i^{obs} are the simulated and observed streamflow at time i.

NSE is expressed by

$$\text{NSE} = 1 - \frac{\sum_{i=1}^{n}\left(Q_i^{sim} - Q_i^{obs}\right)^2}{\sum_{i=1}^{n}\left(Q_i^{obs} - \overline{Q}^{obs}\right)^2}, \tag{15}$$

where $\overline{Q}^{obs}$ indicates the mean value of the measured streamflow for the whole period. This NSE expression puts more importance on high flow. In order to give more weight to low flow, a modified version of the Nash–Sutcliffe coefficient of efficiency is adopted. It is actually a calculation of the NSE in a logarithmic form of the variable (NSE_{log}):

$$\text{NSE}_{log} = 1 - \frac{\sum_{i=1}^{n}\left(\log Q_i^{sim} - \log Q_i^{obs}\right)^2}{\sum_{i=1}^{n}\left(\log Q_i^{obs} - \log\overline{Q}^{obs}\right)^2}. \tag{16}$$

EFF reflects the data assimilation effects by comparing the sum of square error between the streamflow under assimilated and nonassimilated cases. It can be expressed as

$$\text{EFF}(\%) = 100 \cdot \left(1 - \frac{\sum_{i=1}^{n}\left(Q_i^{EnKF} - Q_i^{obs}\right)^2}{\sum_{i=1}^{n}\left(Q_i^{EnOL} - Q_i^{obs}\right)^2}\right), \tag{17}$$

where Q_i^{EnKF} and Q_i^{EnOL} are the predicted streamflow under assimilated and nonassimilated cases at time i.

NER is expressed by the following [55]:

$$\text{NER}(\%) = 100 \cdot \left(1.0 - \frac{\text{RMSE}_{EnKF}}{\text{RMSE}_{EnOL}}\right), \tag{18}$$

where RMSE_{EnKF} and RMSE_{EnOL} are the root mean square errors of the variable in EnKF and EnOL (detailed in Section 4), respectively. The expression for RMSE and R can be found in the study of Liu et al. [56]. The EFF and

Table 2: SWAT model parameters being calibrated.

Sensitivity sequence	Parameters	Description
1	CN_2	SCS curve number for moisture conditon II
2	surlag	Surface runoff lag coefficient
3	α_{gw}	Baseflow recession constant
4	K_{ch}	Effective hydraulic conductivity
5	*esco*	Soil evaporation compensation constant
6	$aq_{shthr,q}$	Threshold depth of water in the shallow aquifer required for the return flow to occur
7	SOL_AWC	Available soil water capacity
8	N	Manning's n value for the main channel
9	can_{mx}	Maximum amount of water that can be trapped in the canopy when that canopy is fully developed
10	*epco*	Plant uptake compensation factor
11	β_{rev}	Revap coefficient
12	δ_{gw}	Delay time for aquifer recharge

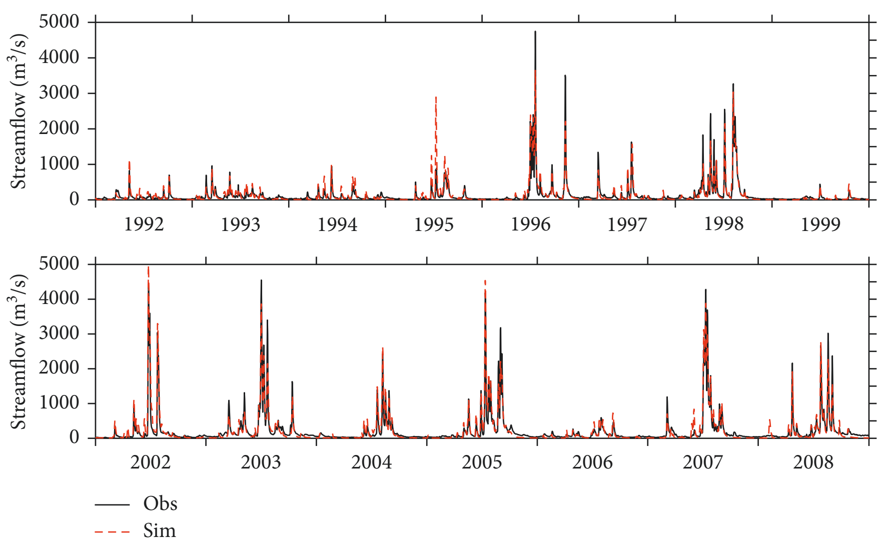

Figure 4: The observed (Obs) and simulated (Sim) daily runoff at the outlet (Huaibin) of the upper Huai River basin over the calibration (1992–1999) and validation (2002–2008) periods.

NER > 0 means that the DA performance is effective. The larger EFF and NER values indicate the better performance of DA.

4. Results

The efficiency of ESA CCI SM assimilation is highly dependent on the quality of model calibration, model, and observation error estimation. Hence, the ESA CCI SM assimilation effects on streamflow simulation accompanied by the results for model calibration and validation and for model and observation error estimation are analyzed. To illustrate the efficiency of DA, the ensemble open-loop (EnOL) cases and the EnKF cases are compared. The EnOL is an ensemble running of the SWAT model with perturbations on model inputs, model parameters, and model states without the integration of observed SM, while the EnKF is an ensemble running of the SWAT model with the same perturbation to EnOL, but with the integration of ESA CCI SM during the model propagation process.

4.1. Model Calibration and Validation. Table 2 presents the SWAT model parameters being calibrated, which are obtained from the parameter sensitivity analysis detailed in Section 3.3.1. Figure 4 plots the simulated and observed daily series of runoff at the catchment outlet during the calibration (1992–1999) and validation (2002–2008) periods. The hydrograph of the simulated streamflow is highly consistent with that of the observed streamflow for both the calibration and validation stages, although slight underestimation exists in flood peak modeling over some periods. The statistics (Table 3) for the simulated streamflow at the catchment outlet (Huaibin) suggest that it agrees well with the measured runoff as RE < 5%, NSE > 0.8, and $R > 0.9$. In addition, the statistics for the other five hydrological sites (Dapoling, Changtaiguan, Zhuganfu, Xixian, and Huangchuan) also indicate that the SWAT model has fairly good applicability in the upper Huai River basin. In the calibration stage, for all six stations, RE < 15%, NSE falls between 0.65~0.81, and $R > 0.83$. In the validation state, RE < 15%, NSE falls between

Table 3: Statistical comparison of the observed and simulated daily runoff over the calibration (1992–1999) and validation (2002–2008) periods.

Hydrologic station	Calibration (1992–1999)				Validation (2002–2008)			
	RE (%)	RMSE (m^3/s)	NSE	R	RE (%)	RMSE (m^3/s)	NSE	R
Dapoling	12.97	28.06	0.66	0.84	15.14	35.49	0.81	0.91
Changtaiguan	−0.74	47.59	0.69	0.85	6.21	63.27	0.78	0.89
Zhuganfu	−7.74	38.53	0.64	0.83	−13.29	51.29	0.69	0.83
Xixian	−1.65	115.84	0.75	0.88	2.24	173.05	0.75	0.88
Huangchuan	0.13	39.61	0.67	0.83	9.89	68.32	0.42	0.73
Huaibin	3.56	133.74	0.81	0.91	1.74	154.13	0.9	0.95

0.69~0.9 (except for Huangchuan), and $R > 0.83$. The unexpected NSEs at Huangchuan are caused by the serious disturbances of the human activities (principally the reservoir impacts) on runoff over the years 2004, 2006, and 2008.

4.2. Model Error Estimation for Precipitation and Model Parameter. Figure 5 shows the objective function F (11) with varying standard deviation (SD) of the lognormal multiplicative perturbation on precipitation (σ_p) from 0.05 to 0.5 along with the varying SD of the normal multiplicative perturbation on parameter from 0.1 to 0.5. The objective function F reaches its minimum value when σ_p approximates 0.35, which suggests that, in this case, the simulated outlet streamflow is the best matching to the observed streamflow from its ensemble statistics. However, it can be seen that σ_{par} is not that sensitive to the objective function, and the allotropism or nonuniqueness issue exits in its optimal parameter estimation. Considering the good performance of the SWAT model in the study basin (Section 4.1), the small values of σ_{par} (<0.25) are more credible. Besides, in consideration of the robustness of the EnKF method [45], 0.25 for σ_{par} is adopted. Note that, in this estimation of σ_p and σ_{par}, the observed streamflow at the subbasin outlet is regarded as the truth, that is, the observation error is ignored. In this case, σ_p and σ_{par} are likely to be slightly overestimated.

4.3. ESA CCI SM Error Estimation. Figure 6 shows the standard deviation (SD) of the observation error σ_R^* (13) for the ESA CCI SM at each grid (34 grids in total) within the catchment. The location for 1–34 grids is present in Figure 7. In general, σ_R^* falls between 0.03 and 0.05 m^3/m^3 for all grids, which is consistent with the accuracy of the ESA CCI SM on average (0.04~0.05 m^3/m^3) [57]. At each grid, σ_R^* presents certain ranges (~0.01 m^3/m^3), which is related to the soil moisture dynamic with time changes over 2003–2006. This also indicates the necessity for considering the temporal characteristics of the observation error for RS SM. In addition, σ_R^* shows a considerable difference among different grids. The high σ_R^* mainly appears on grids with the dense forest coverage, for example, the grids 10, 11, 25, 26, 33, and 34, in particular for the grid 33. The dense forest obscures the emitted radiance of the soil surface, which results in large uncertainty to the surface SM retrieval. Besides, major dense forests are distributed over the catchment with high altitudes

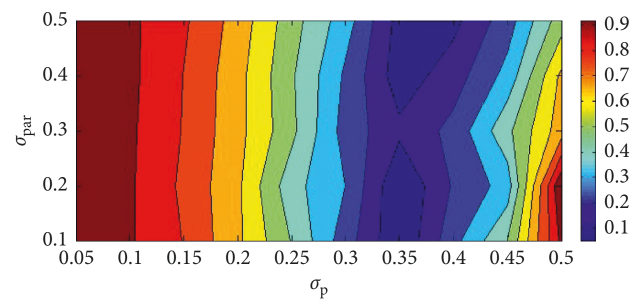

Figure 5: Contour plot of the objective function F (11) with respect to the standard error deviation for precipitation (σ_p) and for model parameter (σ_{par}).

(Figure 1), where the complex topography also impedes the accuracy and reliability of remote sensing for SM [58].

4.4. ESA CCI SM Assimilation on Streamflow Simulation. Table 4 statistically compares the model simulated streamflow with (EnKF) and without (EnOL) ESA CCI SM assimilation at the six hydrologic sites in the upper Huai River basin except for Huangchuan (Figure 1). The reason for Huangchuan not being taken into account is that it has data quality issue over 2004 and 2006 caused by severe human activities. Table 4 shows that the RE and RMSE are decreased and the NSE, NSE_{log}, and R are increased at the five gauges except for Zhuganfu due to ESA CCI soil moisture assimilation. The improvement is more significant in terms of the NSE_{log} as its increase rate is greater than NSE and R, which indicates that the RS soil moisture assimilation is more effective for low flows than high flows. Besides, EFF/NER > 0 for four sites, in particular for Dapoling, Xixian, and Huaibin (where NER > 5% and EFF > 10%), which suggests the good performance of the assimilation. The noneffective performance of ESA CCI SM assimilation on runoff simulation of Changtaiguan and Zhuganfu is probably related to their large proportions of the dense forest and complex topography coverage upstream (Figures 1 and 7). Both dense forest coverage and complex topographical conditions reduce the data quality of RS SM retrievals, thus impeding its performance in DA.

Figure 8 compares the daily series of the model simulated streamflow at the catchment outlet during 2003–2006 with (EnKF) and without (EnOL) ESA CCI SM assimilation on the basis of the observed runoff (Obs). It can be seen that ESA CCI SM assimilation improves the streamflow modeling over low-flow periods. The predicted runoff with ESA CCI SM

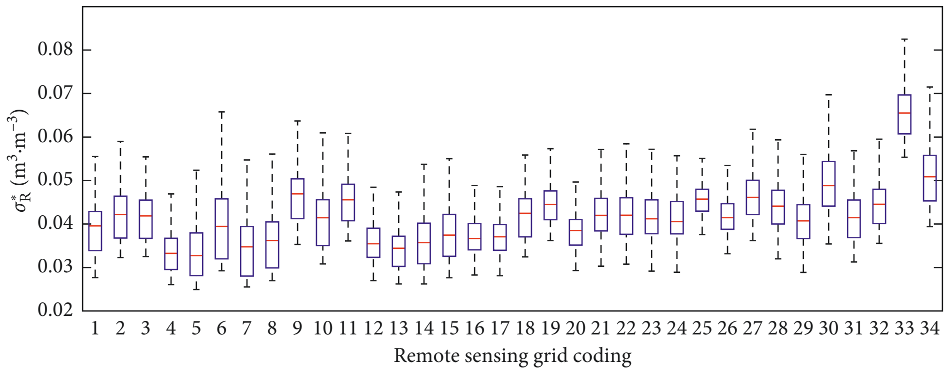

Figure 6: Standard deviation (σ_R^*) of the observation error for the rescaled ESA CCI SM at each grid within the basin. The upper limb, the lower limb, and the red line in the box plot represent the upper quartile (h_1), the lower quartile (h_2), and the median value of σ_R^* over 2003–2006. The dotted line stretched from the box is the range between $h_1 - 1.5\ (h_2 - h_1)$ and $h_2 + 1.5\ (h_2 - h_1)$.

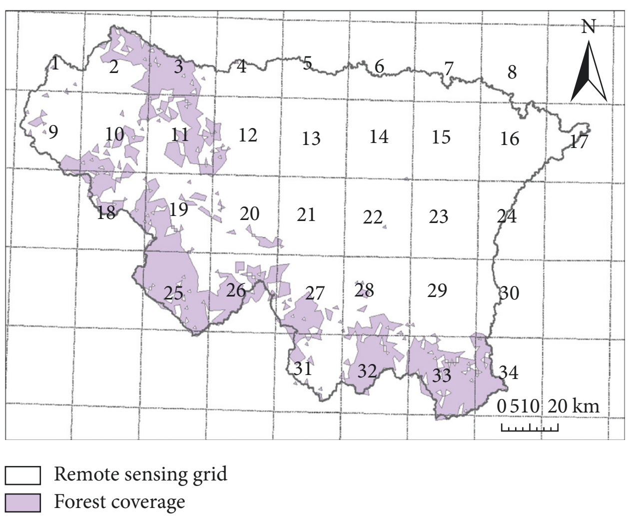

Figure 7: Forest coverage for the remote sensing grids of the ESA CCI SM over the upper Huai River basin. 1–34 is the grid coding for the ESA CCI SM.

assimilation (the red line) is closer to the observed runoff (the black line), and the NSE_{log} increases from 0.6 to 0.71. However, the impact of soil moisture assimilation on streamflow modeling over very high-flow/large-flood periods presents certain uncertainty. For instance, data assimilation improves the streamflow simulation over the periods August 2, 2004–August 12, 2004, and July 3, 2006–July 23, 2006, while it deteriorates the streamflow modeling over the period June 29, 2003–July 9, 2003. These results are consistent with those of the previous researches, for example, the study of Alvarez-Garreton et al. [5] and the study of Massari et al. [32]. The uncertain performance of soil moisture assimilation on large-flood simulation mainly lies in the relatively low dependence of runoff generation on antecedent soil moisture because during large-flood periods, the soil moisture is nearly saturated and the runoff is largely controlled by precipitation inputs.

5. Discussion

In general, our results indicate that the ESA CCI soil moisture assimilation in SWAT performs well in runoff modeling of the whole basin. Streamflow improvements over five in situ sites (except for Zhuganfu) are shown after proper configurations of the model and observation error. However, the improvements are not significant, which can be attributed to the following factors: First, the model error is estimated based on analyzing the ensemble characteristics of the streamflow simulations driven by the model error perturbations in reference to the ground-based runoff observations, during which the observation error for the streamflow is ignored. It might lead to an overestimated model error. In observation error estimation for satellite soil moisture, subjectivity does exist in parameter assignment of the estimation equation although the temporal and spatial variability has been taken into account. These two factors are likely to deteriorate the model and observation error estimation, which eventually degrade the DA performance. Second, the runoff improvements are obtained by updating the profile SM using the satellite SM products, which highly relies on the physical vertical coupling-based model. SWAT soil layers have limited vertical coupling [12, 18] as it does not allow actual soil water compensation from other soil layers in the storage routing technique, and the soil water deficiency is only made up by adjusting the depth distribution of soil evaporation demand. The exponential filter [59] used to derive the profile SM indicator from the surface SM observations is a common solution to the inconsistency of the shallow (surface) RS detection and the runoff root zone control mechanism [5, 32]. However, this approach is more applicable to the hydrological model with a single soil layer setup. For the multilayer setup model (e.g., SWAT), a more promising approach to the physical coupling issue would be adopting Richard's equation because it is more representative of the real-world water movement of soil water. Finally, the runoff improvements show large discrepancies over different hydrological sites with different geographical locations, which suggests that the land surface conditions considerably influence the DA performance (similar to the results from the study of Massari et al. [32]). The dense forests and complex topographical conditions reduce the data quality of microwave soil moisture retrievals, thus deteriorating the efficiency of satellite soil moisture assimilation.

Table 4: Statistical comparison of the estimated streamflow in EnOL and EnKF cases based on the observed streamflow over 2003–2006.

Hydrologic station	EnOL					EnKF					EFF (%)	NER (%)
	RE (%)	RMSE (m^3/s)	NSE	NSE_{log}	R	RE (%)	RMSE (m^3/s)	NSE	NSE_{log}	R		
Dapoling	15.15	35.28	0.82	0.05	0.92	6.65	33	0.84	0.1	0.92	12.51	6.47
Changtaiguan	7.43	61.71	0.78	0.62	0.89	0.09	60.89	0.79	0.68	0.89	2.65	1.33
Zhuganfu	−11.4	43.87	0.67	0.04	0.83	−18.9	44.45	0.66	0.16	0.82	−2.67	−1.3
Xixian	4.1	165	0.74	0.44	0.88	−3.61	156.37	0.77	0.57	0.88	10.19	5.23
Huaibin	5.74	149.9	0.88	0.6	0.94	0.02	140.2	0.9	0.71	0.95	12.47	6.44

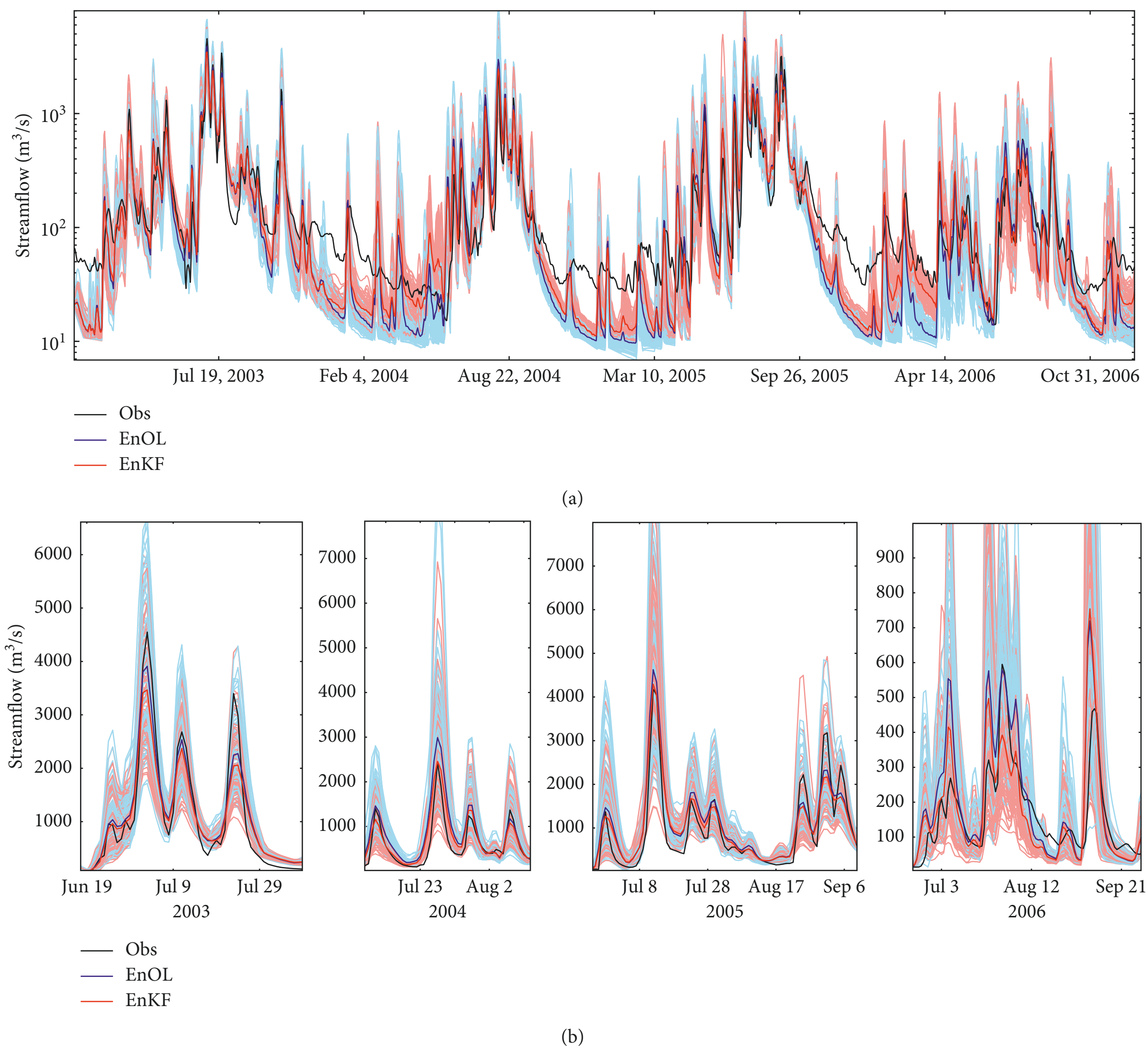

Figure 8: The model-simulated streamflow at the catchment outlet (Huaibin) with (EnKF) and without (EnOL) the ESA CCI SM data assimilation over 2003–2006. The upper plot is for the whole period with a base 10 logarithm coordinate. The four plots below are for the flood season from 2003 to 2006. The red and blue lines are the EnKF and EnOL ensemble members, and the red and blue bold lines represent the mean value of EnKF and EnOL. Obs is the abbreviation of observation.

6. Conclusions

The ESA CCI soil moisture assimilation in the SWAT model using the ensemble Kalman filter (EnKF) with the objective to improve its rainfall-runoff simulation is undertaken in the upper Huai River basin in China. In the assimilation framework, the bias correction for the ESA CCI SM is based on the model-simulated SM using the cumulative distribution function method. The model error is estimated by analyzing the statistical character of the simulated streamflow ensemble under various model error perturbations based on the in situ observed runoff at the catchment outlet. In observation error assessment for the ESA CCI SM, both the spatial heterogeneity and the temporal variability are considered. The observation error is obtained from a linear combination of the minimum retrieval error, the uncertainty indicator in retrieval, and the forest proportions on SM grids. Besides, the SWAT model applicability for the study catchment is assessed before DA as it has significant impacts on the performance of satellite SM assimilation.

The SWAT model has good applicability to the study catchment as the model-simulated daily runoff series are highly consistent with those of the in situ measurements, and the evaluation statistics for all six hydrologic stations are satisfying. In general, the ESA CCI SM assimilation improves the streamflow modeling of the study basin. The DA is more effective for the improvement of low-flow simulation, while for very high-flow/large-flood modeling, the DA performance presents uncertainty. Besides, the DA efficiency is likely to be deteriorated by the dense forest coverage and the complex topographical conditions as it shows large discrepancy over the stations with large and small proportions of the mountainous region at the upstream. Overall, the coarse-scale ESA CCI SM assimilation could improve the streamflow modeling of a physically based semidistributed model, especially for low flow. This study provides an encouragement for the application of the ESA CCI SM in water management over dry seasons or low-flow periods.

Data Availability

The data used to support the findings of this study are available from the corresponding author upon request.

Conflicts of Interest

The authors declare that there are no conflicts of interest regarding the publication of this paper.

Acknowledgments

This work was supported by the State Key Program of National Natural Science Foundation of China (41430855) and the Start-Up Project for Talent Introduction by the Nanjing Institute of Geography & Limnology, Chinese Academy of Sciences (NIGLAS2017QD03).

References

[1] J. P. Walker, G. R. Willgoose, and J. D. Kalma, "One-dimensional soil moisture profile retrieval by assimilation of near-surface observations: a comparison of retrieval algorithms," *Advances in Water Resources*, vol. 24, no. 6, pp. 631–650, 2001.

[2] I. A. Lunt, S. S. Hubbard, and Y. Rubin, "Soil moisture content estimation using ground-penetrating radar reflection data," *Journal of Hydrology*, vol. 307, no. 1–4, pp. 254–269, 2005.

[3] R. H. Reichle, W. T. Crow, and C. L. Keppenne, "An adaptive ensemble Kalman filter for soil moisture data assimilation," *Water Resources Research*, vol. 44, no. 3, p. 006357, 2008.

[4] L. Brocca, T. Moramarco, F. Melone, W. Wagner, S. Hasenauer, and S. Hahn, "Assimilation of surface- and root-zone ASCAT soil moisture products into rainfall–runoff modeling," *IEEE Transactions on Geoscience and Remote Sensing*, vol. 50, pp. 2542–2555, 2012.

[5] C. Alvarez-Garreton, D. Ryu, A. W. Western, W. T. Crow, and D. E. Robertson, "The impacts of assimilating satellite soil moisture into a rainfall–runoff model in a semi-arid catchment," *Journal of hydrology*, vol. 519, pp. 2763–2774, 2014.

[6] C. Alvarez-Garreton, D. Ryu, A. W. Western, W. T. Crow, C. H. Su, and D. R. Robertson, "Dual assimilation of satellite soil moisture to improve streamflow prediction in data-scarce catchments," *Water Resources Research*, vol. 52, no. 7, pp. 5357–5375, 2016.

[7] P. López, N. Wanders, J. Schellekens, L. J. Renzullo, E. H. Sutanudjaja, and M. F. P. Bierkens, "Improved large-scale hydrological modelling through the assimilation of streamflow and downscaled satellite soil moisture observations," *Hydrology and Earth System Sciences Discussions*, vol. 12, no. 10, pp. 10559–10601, 2015.

[8] P. W. Liu, T. Bongiovanni, A. Monsivais-Huertero et al., "Assimilation of active and passive microwave observations for improved estimates of soil moisture and crop growth," *IEEE Journal of Selected Topics in Applied Earth Observations and Remote Sensing*, vol. 9, no. 4, pp. 1357–1369, 2016.

[9] Y. Liu, W. Wang, and Y. Hu, "Investigating the impact of surface soil moisture assimilation on state and parameter estimation in SWAT model based on the ensemble Kalman filter in upper Huai River basin," *Journal of Hydrology and Hydromechanics*, vol. 65, no. 2, pp. 123–133, 2017.

[10] J. Loizu, C. Massari, J. Álvarez-Mozos, A. Tarpanelli, L. Brocca, and J. Casalí, "On the assimilation set-up of ASCAT soil moisture data for improving streamflow catchment simulation," *Advances in Water Resources*, vol. 111, pp. 86–104, 2018.

[11] W. T. Crow and D. Ryu, "A new data assimilation approach for improving runoff prediction using remotely-sensed soil moisture retrievals," *Hydrology and Earth System Sciences*, vol. 13, no. 1, pp. 1–16, 2009.

[12] F. Chen, W. T. Crow, P. J. Starks, and D. N. Moriasi, "Improving hydrologic predictions of a catchment model via assimilation of surface soil moisture," *Advances in Water Resources*, vol. 34, no. 4, pp. 526–536, 2011.

[13] F. Lei, C. Huang, H. Shen, and X. Li, "Improving the estimation of hydrological states in the SWAT model via the ensemble Kalman smoother: synthetic experiments for the Heihe River Basin in northwest China," *Advances in Water Resources*, vol. 67, pp. 32–45, 2014.

[14] W. Chen, C. Huang, H. Shen, and X. Li, "Comparison of ensemble-based state and parameter estimation methods for soil moisture data assimilation," *Advances in Water Resources*, vol. 86, pp. 425–438, 2015.

[15] P. Baguis and E. Roulin, "Soil moisture data assimilation in a hydrological model: a case study in Belgium using large-scale satellite data," *Remote Sensing*, vol. 9, no. 8, p. 820, 2017.

[16] W. T. Crow, F. Chen, R. H. Reichle, and Q. Liu, "L-band microwave remote sensing and land data assimilation improve the representation of pre-storm soil moisture conditions for hydrologic forecasting," *Geophysical Research Letters*, vol. 44, no. 11, pp. 5495–5503, 2017.

[17] H. Lee, D. J. Seo, and V. Koren, "Assimilation of streamflow and in situ soil moisture data into operational distributed hydrologic models: effects of uncertainties in the data and initial model soil moisture states," *Advances in Water Resources*, vol. 34, no. 12, pp. 1597–1615, 2011.

[18] E. Han, V. Merwade, and G. C. Heathman, "Implementation of surface soil moisture data assimilation with watershed scale distributed hydrological model," *Journal of Hydrology*, vol. 416, pp. 98–117, 2012.

[19] C. Albergel, C. Rüdiger, T. Pellarin et al., "From near-surface to root-zone soil moisture using an exponential filter: an assessment of the method based on in-situ observations and model simulations," *Hydrology and Earth System Sciences Discussions*, vol. 12, no. 6, pp. 1323–1337, 2008.

[20] R. H. Reichle and R. D. Koster, "Global assimilation of satellite surface soil moisture retrievals into the NASA Catchment land surface model," *Geophysical Research Letters*, vol. 32, no. 2, 2005.

[21] R. H. Reichle, R. D. Koster, P. Liu, S. P. Mahanama, E. G. Njoku, and M. Owe, "Comparison and assimilation of global soil moisture retrievals from the advanced microwave scanning radiometer for the earth observing system (AMSR-E) and the scanning multichannel microwave radiometer (SMMR)," *Journal of Geophysical Research: Atmospheres*, vol. 112, no. D9, 2007.

[22] W. T. Crow and R. H. Reichle, "Comparison of adaptive filtering techniques for land surface data assimilation," *Water Resources Research*, vol. 44, no. 8, 2008.

[23] C. Huang, X. Li, L. Lu, and J. Gu, "Experiments of one-dimensional soil moisture assimilation system based on ensemble Kalman filter," *Remote Sensing of Environment*, vol. 112, no. 3, pp. 888–900, 2008.

[24] D. Ryu, W. T. Crow, X. Zhan, and T. J. Jackson, "Correcting unintended perturbation biases in hydrologic data assimilation," *Journal of Hydrometeorology*, vol. 10, no. 3, pp. 734–750, 2009.

[25] G. Wu, B. Dan, and X. Zheng, "Soil moisture assimilation using a modified ensemble transform Kalman filter based on station observations in the Hai River Basin," *Advances in Meteorology*, vol. 2016, Article ID 4569218, 12 pages, 2016.

[26] D. Liu and A. K. Mishra, "Performance of AMSR_E soil moisture data assimilation in CLM4 model for monitoring hydrologic fluxes at global scale," *Journal of hydrology*, vol. 547, pp. 67–79, 2017.

[27] L. Brocca, F. Melone, T. Moramarco et al., "Improving runoff prediction through the assimilation of the ASCAT soil moisture product," *Hydrology and Earth System Sciences*, vol. 14, no. 10, pp. 1881–1893, 2010.

[28] F. Chen, W. T. Crow, and D. Ryu, "Dual forcing and state correction via soil moisture assimilation for improved rainfall–runoff modeling," *Journal of Hydrometeorology*, vol. 15, no. 5, pp. 1832–1848, 2014.

[29] P. Laiolo, S. Gabellani, L. Campo et al., "Impact of different satellite soil moisture products on the predictions of a continuous distributed hydrological model," *International Journal of Applied Earth Observation and Geoinformation*, vol. 48, pp. 131–145, 2016.

[30] H. Lievens, S. K. Tomer, A. Al Bitar et al., "SMOS soil moisture assimilation for improved hydrologic simulation in the Murray Darling Basin, Australia," *Remote Sensing of Environment*, vol. 168, pp. 146–162, 2015.

[31] C. Massari, S. Camici, L. Ciabatta, and L. Brocca, "Exploiting satellite-based surface soil moisture for flood forecasting in the Mediterranean area: state update versus rainfall correction," *Remote Sensing*, vol. 10, no. 2, p. 292, 2018.

[32] C. Massari, L. Brocca, A. Tarpanelli, and T. Moramarco, "Data assimilation of satellite soil moisture into rainfall-runoff modelling: a complex recipe?," *Remote Sensing*, vol. 7, no. 9, pp. 11403–11433, 2015.

[33] M. Rodell, P. R. Houser, U. E. A. Jambor et al., "The global land data assimilation system," *Bulletin of the American Meteorological Society*, vol. 85, no. 3, pp. 381–394, 2004.

[34] W. Wagner, W. Dorigo, R. de Jeu et al., "Fusion of active and passive microwave observations to create an essential climate variable data record on soil moisture," *ISPRS Annals of the Photogrammetry, Remote Sensing and Spatial Information Sciences (ISPRS Annals)*, vol. 7, pp. 315–321, 2012.

[35] X. Xie, S. Meng, S. Liang, and Y. Yao, "Improving streamflow predictions at ungauged locations with real-time updating: application of an EnKF-based state-parameter estimation strategy," *Hydrology and Earth System Sciences*, vol. 18, no. 10, pp. 3923–3936, 2014.

[36] T. Worku, D. Khare, and S. K. Tripathi, "Modeling runoff–sediment response to land use/land cover changes using integrated GIS and SWAT model in the Beressa watershed," *Environmental Earth Sciences*, vol. 76, no. 16, p. 550, 2017.

[37] Soil Conservation Service, "Section 4: hydrology," in *National Engineering Handbook*, SCS, Washington, DC, USA, 1972.

[38] J. L. Monteith, Evaporation and environment, "Symposia of the Society for Experimental Biology," vol. 19, no. 205–223, p. 4, 1965.

[39] S. L. Neitsch, J. G. Arnold, J. R. Kiniry, and J. R. Williams, *Soil and Water Assessment Tool Theoretical Documentation Version 2009*, Texas Water Resources Institute, College Station, TX, USA, 2011.

[40] J. Williams, "Flood routing with variable travel time or variable storage coefficients," *Transactions of the ASAE*, vol. 12, no. 1, pp. 100–103, 1969.

[41] G. Evensen, "Sequential data assimilation with a nonlinear quasi-geostrophic model using Monte Carlo methods to forecast error statistics," *Journal of Geophysical Research: Oceans*, vol. 99, no. C5, pp. 10143–10162, 1994.

[42] M. D. McKay, R. J. Beckman, and W. J. Conover, "Comparison of three methods for selecting values of input variables in the analysis of output from a computer code," *Technometrics*, vol. 21, no. 2, pp. 239–245, 1979.

[43] M. D. Morris, "Factorial sampling plans for preliminary computational experiments," *Technometrics*, vol. 33, no. 2, pp. 161–174, 1991.

[44] K. Abbaspour, C. Johnson, and M. T. Van Genuchten, "Estimating uncertain flow and transport parameters using a sequential uncertainty fitting procedure," *Vadose Zone Journal*, vol. 3, no. 4, pp. 1340–1352, 2004.

[45] X. Xie and D. Zhang, "Data assimilation for distributed hydrological catchment modeling via ensemble Kalman filter," *Advances in Water Resources*, vol. 33, no. 6, pp. 678–690, 2010.

[46] J. Dong, S. C. Steele-Dunne, J. Judge, and N. van de Giesen, "A particle batch smoother for soil moisture estimation using soil temperature observations," *Advances in Water Resources*, vol. 83, pp. 111–122, 2015.

[47] D. P. Dee and A. M. Da Silva, "Data assimilation in the presence of forecast bias," *Quarterly Journal of the Royal Meteorological Society*, vol. 124, no. 545, pp. 269–295, 1998.

[48] R. H. Reichle and R. D. Koster, "Bias reduction in short records of satellite soil moisture," *Geophysical Research Letters*, vol. 31, no. 19, 2004.

[49] H. M. Barré, B. Duesmann, and Y. H. Kerr, "SMOS: the mission and the system," *IEEE Transactions on Geoscience and Remote Sensing*, vol. 46, no. 3, pp. 587–593, 2008.

[50] D. Entekhabi, E. G. Njoku, P. E. O'Neill et al., "The soil moisture active passive (SMAP) mission," *Proceedings of the IEEE*, vol. 98, no. 5, pp. 704–716, 2010.

[51] W. T. Crow, R. Bindlish, and T. J. Jackson, "The added value of spaceborne passive microwave soil moisture retrievals for

forecasting rainfall-runoff partitioning," *Geophysical Research Letters*, vol. 32, no. 18, 2005.
[52] J. Dong and W. T. Crow, "An improved triple collocation analysis algorithm for decomposing autocorrelated and white soil moisture retrieval errors," *Journal of Geophysical Research: Atmospheres*, vol. 122, no. 24, pp. 13081–13094, 2017.
[53] Y. Y. Liu, R. M. Parinussa, W. A. Dorigo et al., "Developing an improved soil moisture dataset by blending passive and active microwave satellite-based retrievals," *Hydrology and Earth System Sciences*, vol. 15, no. 2, p. 425, 2011.
[54] Y. Y. Liu, R. A. de Jeu, M. F. McCabe, J. P. Evans, and A. I. van Dijk, "Global long-term passive microwave satellite-based retrievals of vegetation optical depth," *Geophysical Research Letters*, vol. 38, no. 18, 2011.
[55] H. Chen, D. Yang, Y. Hong, J. J. Gourley, and Y. Zhang, "Hydrological data assimilation with the ensemble square-root-filter: use of streamflow observations to update model states for real-time flash flood forecasting," *Advances in Water Resources*, vol. 59, pp. 209–220, 2013.
[56] Y. Liu, W. Wang, Y. Hu, and W. Cui, "Improving the distributed hydrological model performance in upper Huai River basin: using streamflow observations to update the basin states via the ensemble Kalman filter," *Advances in Meteorology*, vol. 2016, Article ID 4921616, 14 pages, 2016.
[57] W. A. Dorigo, A. Gruber, R. A. M. De Jeu et al., "Evaluation of the ESA CCI soil moisture product using ground-based observations," *Remote Sensing of Environment*, vol. 162, pp. 380–395, 2015.
[58] E. G. Njoku, T. J. Jackson, V. Lakshmi, T. K. Chan, and S. V. Nghiem, "Soil moisture retrieval from AMSR-E," *IEEE Transactions on Geoscience and Remote Sensing*, vol. 41, no. 2, pp. 215–229, 2003.
[59] W. Wagner, G. Lemoine, and H. Rott, "A method for estimating soil moisture from ERS scatterometer and soil data," *Remote Sensing of Environment*, vol. 70, no. 2, pp. 191–207, 1999.